

Geophysical Research Letters®

RESEARCH LETTER

10.1029/2021GL096465

Key Points:

- Using Envisat InSAR and GNSS data, we derive a velocity field derived for New Zealand
- Combining InSAR and GNSS enables us to provide a nationwide estimate of the vertical deformation field for the first time
- Estimated vertical rates show large variability around the country as a result of volcanic, tectonic, and anthropogenic sources

Supporting Information:

Supporting Information may be found in the online version of this article.

Correspondence to:

I. J. Hamling,
I.Hamling@gns.cri.nz

Citation:

Hamling, I. J., Wright, T. J., Hreinsdóttir, S., & Wallace, L. M. (2022). A snapshot of New Zealand's dynamic deformation field from Envisat InSAR and GNSS observations between 2003 and 2011. *Geophysical Research Letters*, 49, e2021GL096465. <https://doi.org/10.1029/2021GL096465>

Received 6 OCT 2021
Accepted 6 DEC 2021

A Snapshot of New Zealand's Dynamic Deformation Field From Envisat InSAR and GNSS Observations Between 2003 and 2011

Ian J. Hamling¹ , Tim J. Wright² , Sigrun Hreinsdóttir¹ , and Laura M. Wallace^{1,3} 

¹GNS Science, Lower Hutt, New Zealand, ²School of Earth and Environment, University of Leeds, Leeds, UK, ³University of Austin at Texas, Austin, TX, USA

Abstract Measuring the deformation at the Earth's surface over a range of spatial and temporal scales is vital for understanding seismic hazard, detecting volcanic unrest, and assessing the effects of vertical land movements (VLMs) on sea level rise. Here, we combine ~10 years of Interferometric Synthetic Aperture Radar (InSAR) observations from Envisat with interseismic campaign and continuous GNSS velocities to build a high-resolution velocity field of New Zealand. Exploiting the horizontal GNSS observations, we estimate the vertical component of the deformation to provide the VLM for the entire 15,000-km-long coastline. The estimated vertical rates show large variability around the country as a result of volcanic, tectonic, and anthropogenic sources. Interseismic subsidence is observed in Kaikoura region supporting models of at least partial locking of the southern Hikurangi subduction interface. Despite data challenges in the mountainous regions from landslides, sediment compaction, and glaciers, InSAR data shows localized uplift of the Southern Alps.

Plain Language Summary Interferometric Synthetic Aperture Radar (InSAR) data provides a method to measure the deformation of the Earth's surface at high spatial resolutions over large geographic footprints. Here we exploit historical SAR and GNSS data acquired over New Zealand between 2003 and 2011 to measure the nationwide surface velocities. With the combination of GNSS and InSAR data, we are able to estimate the vertical deformation for the entire country and provide a first estimate of the coastal vertical land movements which are a key data set for future projections of sea level rise. As a result of New Zealand's dynamic tectonic setting, there is large temporal and spatial variability around the country as a result of volcanic, tectonic, and anthropogenic processes.

1. Introduction

From mapping the build-up and release of strain associated with the earthquake cycle (Cavalié et al., 2008; Haines & Wallace, 2020; H. Wang et al., 2012; Weiss et al., 2020) to tracking the movement of magma in volcanic systems (Biggs & Wright, 2020; Ebmeier et al., 2018; Hamling et al., 2019; Pritchard & Simons, 2002), geodetic observations have become powerful tools for studying the deformation of the Earth's crust over a range of spatial and temporal scales. While GNSS data can provide high precision (mm/yr) measurements of the deformation field, the low-density of observation points (typically >10 km) frequently limits our ability to resolve short wavelength variations in land movements. Since 1992 and the development of GNSS networks in New Zealand, there have been numerous efforts to measure and model the velocity field across New Zealand (Beavan & Haines, 2001; Beavan et al., 2016; Wallace et al., 2004, 2007). While the current campaign and continuous network provides comprehensive coverage of both islands, with a spacing of 10–20 km and repeat campaign measurements every 8 years, resolving short wavelength deformation signals remains challenging. Furthermore, since the early 2000s, New Zealand has been rocked by numerous M_w 6.5 and larger earthquakes (Beavan et al., 2012; Beavan, Samsonov, et al., 2010; Hamling et al., 2014, 2017; Hamling & Hreinsdóttir, 2016; Reyners et al., 2003) adding additional uncertainty in estimating the interseismic velocity field. Here we present a new Interferometric Synthetic Aperture Radar (InSAR) derived velocity field based on historic Envisat data acquired between 2003 and 2010, largely spanning a time period isolated from some of the larger earthquake sequences.

Across New Zealand, the oblique convergence between the Pacific and Australian plates at rates of ~30–40 mm/yr has resulted in a complex plate boundary with large along strike variations in tectonic regimes. In the North Island, the tectonics are dominated by the westward subduction of the Pacific plate along the Hikurangi trough

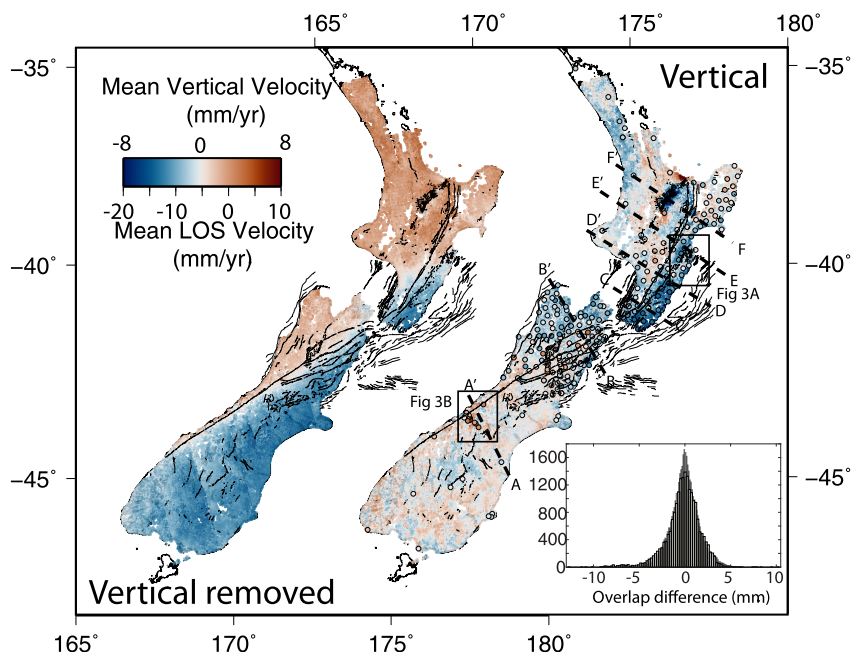


Figure 1. Best fitting LOS (left) and vertical (right) displacement rates. The figure shows a subsampled version of the full data set derived using a distance weighted sampling procedure. The histogram shows the difference in rates within all the overlap regions for the North and south Islands. The black lines show the location of mapped faults (Langridge et al., 2016). On the right-hand panel, dashed lines show the location of the profiles shown in Figure 2 and the black boxes show the regions in Figure 3. The colored dots are the vertical rates derived from GNSS covering the same observation period.

(Wallace & Beavan, 2010). While the normal component of plate motion is accommodated along the subduction thrust and shortening within the overriding plate (Nicol & Beavan, 2003), the margin parallel component is accommodated via strike-slip faulting and rotation of the forearc (Wallace et al., 2004). Along the Hikurangi margin, block modeling of campaign GNSS data suggests a transition from aseismic creep in the north to interseismic coupling in the south down to depths of 30–40 km (Wallace, Barnes, et al., 2012; Wallace, Beavan, et al., 2012). Slow slip events (SSEs) have been well documented beneath and offshore the North Island in a number of locations (Hamling & Wallace, 2015; Wallace & Beavan, 2010; Wallace, Beavan, et al., 2012; Wallace, 2020), with periodicities ranging from weeks to years. More frequently occurring, but shorter duration, SSEs are located along the northern margin and largely occur along the offshore portion of the plate boundary. Conversely, SSEs at the southern and central Hikurangi margin are deeper and typically last for periods of years and have previously been captured by InSAR data (Hamling & Wallace, 2015).

In the northern South Island, ~80% of plate motion is taken up along four major strike-slip faults through the Marlborough Fault system (Holt & Haines, 1995; Van Dissen & Yeats, 1991) with increasing slip rates from ~4 mm/yr in the north to ~23 mm/yr in the south along the Hope Fault (Langridge & Berryman, 2005; Van Dissen & Yeats, 1991; Wallace et al., 2007). The region has been struck by a number of moderate to large earthquakes over the last 10 years, including the 2013 Cook Strait and Lake Grassmere sequence (Hamling et al., 2014) and the 2016 Kaikōura earthquake which ruptured multiple faults through area. South of the Marlborough fault system, 70%–75% of the Pacific-Australia relative motion is taken up along the Alpine Fault with the remainder accommodated across the South Island (Wallace et al., 2007). The convergent component of motion has led to the growth of the Southern Alps (Norris & Cooper, 2001; Sutherland et al., 2006) which, in the central portion, has experienced long-term exhumation at rates of 6–9 mm/yr (Little et al., 2005; Michailos et al., 2020) with current estimates from geodetic data suggesting lower rates of ~5 mm/yr (Beavan, Denys, et al., 2010; Beavan et al., 1999). Further south, the zone of deformation broadens from ~70 km in the Canterbury region to ~200 km across Central Otago (Figure 1) and has been explained by along strike rheological variations (Upton & Koons, 2007; Upton et al., 2009).

2. SAR Observations

Between 2003 and 2011, the European Space Agency's Envisat satellite captured ~700 SAR scenes covering the North and South Islands of New Zealand across 20 ascending tracks (Figures S1–S6 in Supporting Information S1). The SW plate motion across most of New Zealand is well orientated with respect to the geometry of the ascending tracks and while the temporal sampling and number of images per track were variable, most had ~20 scenes over the ~8 years observation period. Unfortunately, only limited descending data were acquired across New Zealand making it largely unusable for deriving a long-term rate. For the ascending data, we use the StaMPS (Stanford Method for Persistent Scatterers) small baseline time series technique (Hooper, 2008; Hooper et al., 2012) to form ~2,700 interferograms across the 20 tracks. SAR data were initially focused using the JPL/Caltech ROI_PAC software (Rosen et al., 2004) and interferograms were made using DORIS (Kampes et al., 2003). Topographic corrections were made using a 1 arc-second (30 m) digital elevation model (DEM) generated by the NASA Shuttle Radar Topography Mission (Farr et al., 2007). To minimize phase unwrapping errors, we apply an iterative unwrapping algorithm (Hussain et al., 2016) which utilizes the standard StaMPS unwrapping method but calculates the sum of the unwrapped phase around closed loops for every coherent pixel (Hussain et al., 2016). With large M_w 7.8 and 7.2 earthquakes in Fiordland (2009) and Darfield (2010), respectively (Figure 1), interferograms spanning these events were dropped from the analysis.

To estimate the interseismic velocity field, we adopted two slightly different procedures for the North and South Islands. For both Islands, to prevent the removal of the expected long wavelength interseismic deformation and help with the correction of non-tectonic signals, including orbits and long wavelength atmospheric errors, we first removed the expected horizontal component of the velocity field from each interferogram using the velocity field extracted from the Vertical Derivatives of Horizontal Stress (VdoHS) rate inversion derived by (Haines & Wallace, 2020). Although this is calculated using continuous and campaign data (Beavan et al., 2016) over a longer period than the InSAR observations, the difference between the long term and InSAR period velocities are negligible (Figure S7 in Supporting Information S1). For the top of the South Island and North Island, due to the larger expected vertical deformation and better continuous GPS coverage, we also estimated the vertical rate at GNSS with data spanning the same period as the InSAR observations (Supporting Information). We then removed the vertical component from each interferogram by fitting a cubic plane through the vertical GNSS data (Figure S8 in Supporting Information S1). For the remainder of the South Island, where there are insufficient GNSS observations to robustly extrapolate the vertical deformation field, we did not remove any a priori model. Due to large vertical deformation through the Taupo Volcanic Zone into the Bay of Plenty (Figure 1; Hamling et al., 2015, 2016), we also removed the vertical deformation based on the contraction model of (Hamling et al., 2015; Figure S8 in Supporting Information S1). We then used the remaining data to estimate and remove orbital and atmospheric errors. To separate the vertical and horizontal components of the velocity field, we perform two inversions. In the first, after correcting the interferograms, we added back the GNSS derived horizontal velocities and, using a linear least-squares inversion, we solved for the best fitting displacement rate, \mathbf{x} , at each scatterer such that

$$\mathbf{A}^T \Sigma^{-1} \mathbf{A} \mathbf{x} = \mathbf{A}^T \Sigma^{-1} \mathbf{d}. \quad (1)$$

where the design matrix, \mathbf{A} , contains the time interval of each interferogram, \mathbf{d} is a matrix containing the displacements at each scatterer, and Σ is the variance-covariance matrix. In the second inversion, to isolate the vertical component of the deformation field, we only add the vertical components back to the interferograms and assume that after removal of the horizontal component, the residual deformation is representative of the vertical deformation field (Figure 1). For the final rate maps, we removed scatterers deemed to be outliers based on the estimated vertical rates. For each scatterer in the data set ($\sim 3 \times 10^6$), we first calculated the mean absolute deviation of all neighboring scatterers within a 1 km radius. If a scatterer had a standard deviation of more than 2σ , it was deemed an outlier and given a score of 1. The process is repeated through the entire data set and scatterers which are identified as being outliers more than 10% of the time are removed. This reduces the final data set by ~30% to $\sim 2 \times 10^6$ points.

To check for consistency between tracks, we compared the estimated displacement rates in the overlap regions between the frames and with the GNSS velocities at collocated sites (Figures 1 and S9 in Supporting Information S1). There is a good match between the InSAR derived displacement rates in the overlap regions with a mean difference and standard deviation of -0.05 and 1.6 mm/yr, respectively (Figures 1 and S10 in Supporting

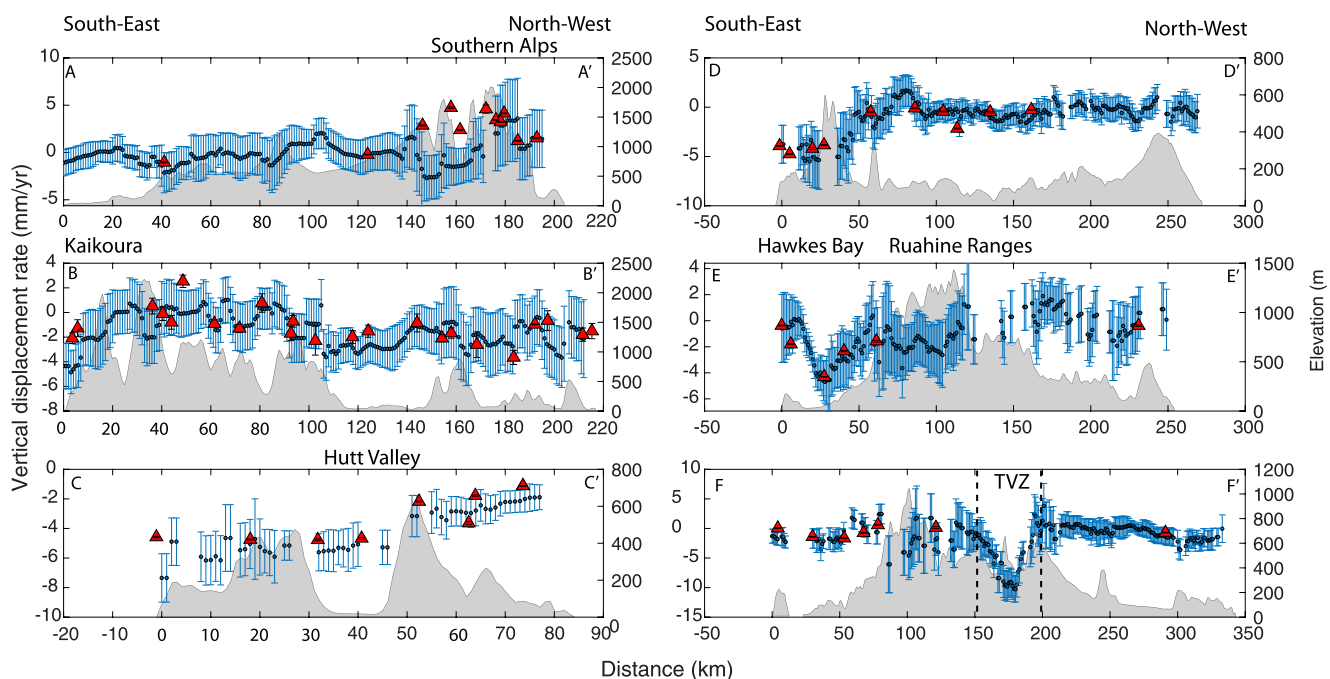


Figure 2. Profiles along six profiles shown in Figure 1. Blue dots and associated error bars are from the InSAR derived vertical velocities and the red dots are from GNSS located within 10 km of the profile. The gray polygons show the topography along each of the profiles. Locations, including Kaikōura, the Southern Alps and the TVZ are also highlighted.

Information S1). The mean difference and standard deviation between the horizontal component of the velocity field from GNSS and InSAR are 0.03 and 1.1 mm/yr, respectively.

3. Discussion

3.1. North Island

Across the North Island, both InSAR and GNSS data are dominated by the clockwise rotation of the fore-arc and the effect of interseismic coupling on the southern Hikurangi subduction interface shown by the \sim 15 mm/yr LOS displacement rates through the southern North Island (Figure 2). In the central North Island, deformation is strongly influenced by the TVZ. Earlier studies (Hamling et al., 2015; Holden et al., 2015) have shown that the deformation is largely in the vertical component leading to some horizontal contraction (Figure 1; Haines & Wallace, 2020). Subsidence of 10–15 mm/yr is observed through the central TVZ extending from Lake Taupo to the Okataina caldera in the north with more focused subsidence over some of the active geothermal fields. The large-scale subsidence has previously been attributed to the cooling and contraction of pockets of magma at depth (Hamling et al., 2015; Holden et al., 2015) or from the deep upwelling of mantle material (Lamb et al., 2017). During the observation period, there was uplift in the Lake Taupo region in the central/southern TVZ, and the Bay of Plenty region at the northern end. Unrest in the vicinity of Taupo caused a period of uplift in 2008 focused around the northern tip of the lake which is also captured by the InSAR observations (Figure 1). In the Bay of Plenty, a \sim 30 km wide zone of uplift between 2005 and 2011 along the coast has been attributed to an off-axis magma body undergoing a pulse of inflation (Hamling et al., 2016).

Much of the north and west coasts of the North Island are relatively stable with slight subsidence of \sim 1 mm/yr predicted in the vicinity of New Zealand's largest city, Auckland. Along the east coast, InSAR and GNSS both indicate widespread subsidence increasing in magnitude from Hawkes Bay in the north toward Cook Strait in the south consistent with the inferred locking along the subduction interface (Wallace, Barnes, et al., 2012; Wallace et al., 2004; Figure 1). Within Hawkes Bay, the InSAR derived rates highlight short wavelength variations in the vertical deformation. Subsidence of \sim 5 mm/yr in the vicinity of Napier extends inland through the Heretaunga Plains and is bounded to the south east by the Maraetotara Plateau and to the north west by the North

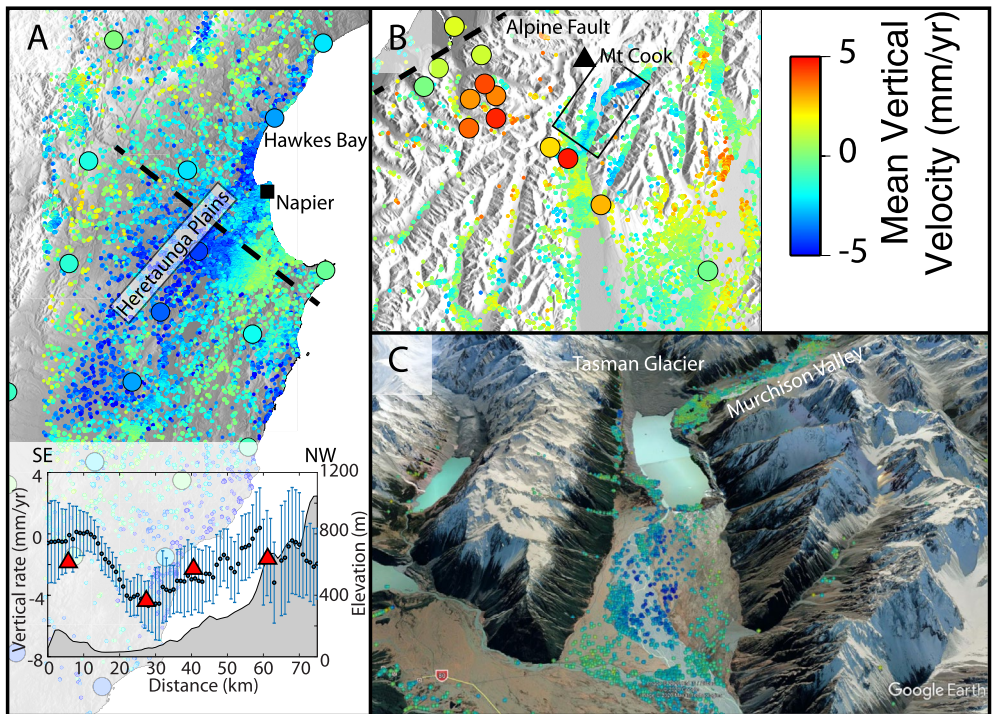


Figure 3. (a) Zoom-in of the vertical deformation across Hawkes Bay and the Heretaunga Plains and profile showing the sharp transition to subsidence. (b) Zoom-in of the central Southern Alps highlighting the non-tectonic deformation along some of the glacial river valleys. The black triangle shows the location of Aoraki/Mt Cook (170.177 E, -43.585 S). The black dashed line shows the location of the Alpine Fault, the black box shows the region covered in (c) and the colored circles are the GNSS derived vertical rates.

Island dextral fault belt (Figures 2 and 3). Based on the horizontal velocity field, VDoHS strain rates (Dimitrova et al., 2016; Haines & Wallace, 2020) show a local zone of contraction which has been explained as a possible locked patch on the subduction interface at the central Hikurangi margin (Dimitrova et al., 2016). Although the plate interface is only ~15–20 km deep, the fairly sharp transition to subsidence (Figure 3a) may indicate a shallower crustal source pointing toward partitioning of strain from the interface onto overlying crustal faults or a combination of subduction locking and crustal faulting sources. Additionally, shallow groundwater abstraction from across the plains is likely to contribute to some of the subsidence signal.

3.2. South Island

While data across the South Island successfully captures the large-scale right-lateral motion across the plate boundary (Figure 1), the estimated vertical velocities have larger uncertainties. Challenges in deriving the InSAR velocity field stem from the limited distribution of scatterers and contamination from non-tectonic signals. In the mountainous regions, which form the backbone of the South Island, a combination of snow cover, dense vegetation, and steep terrain often restrict the distribution of scatterers to exposed slopes. These are often associated with past debris falls or landslides, or within rapidly changing glacial river valleys (Figure 3). This is especially problematic when looking at the vertical component of the deformation field where the expected displacement rates are an order of magnitude smaller than the horizontal component (Figure 1). Scatterers located on downward facing slopes, relative to the ascending look direction, often indicate motion away from the satellite suggesting either subsidence or downslope motion consistent with landsliding (Figures 1 and 3). We also observe complex displacement patterns in the vicinity of the Tasman glacier. Continuous GNSS data in the region suggests uplift of the Southern Alps by ~5 mm/yr (Beavan, Denys, et al., 2010). However, near the outflow of Lake Tasman at the base of the Tasman Glacier (Figure 4), subsidence of ~3–5 mm/yr is observed over a ~3 km² area with a similar pattern observed along the connecting Murchison valley (Figure 3). While the source of the subsidence is not

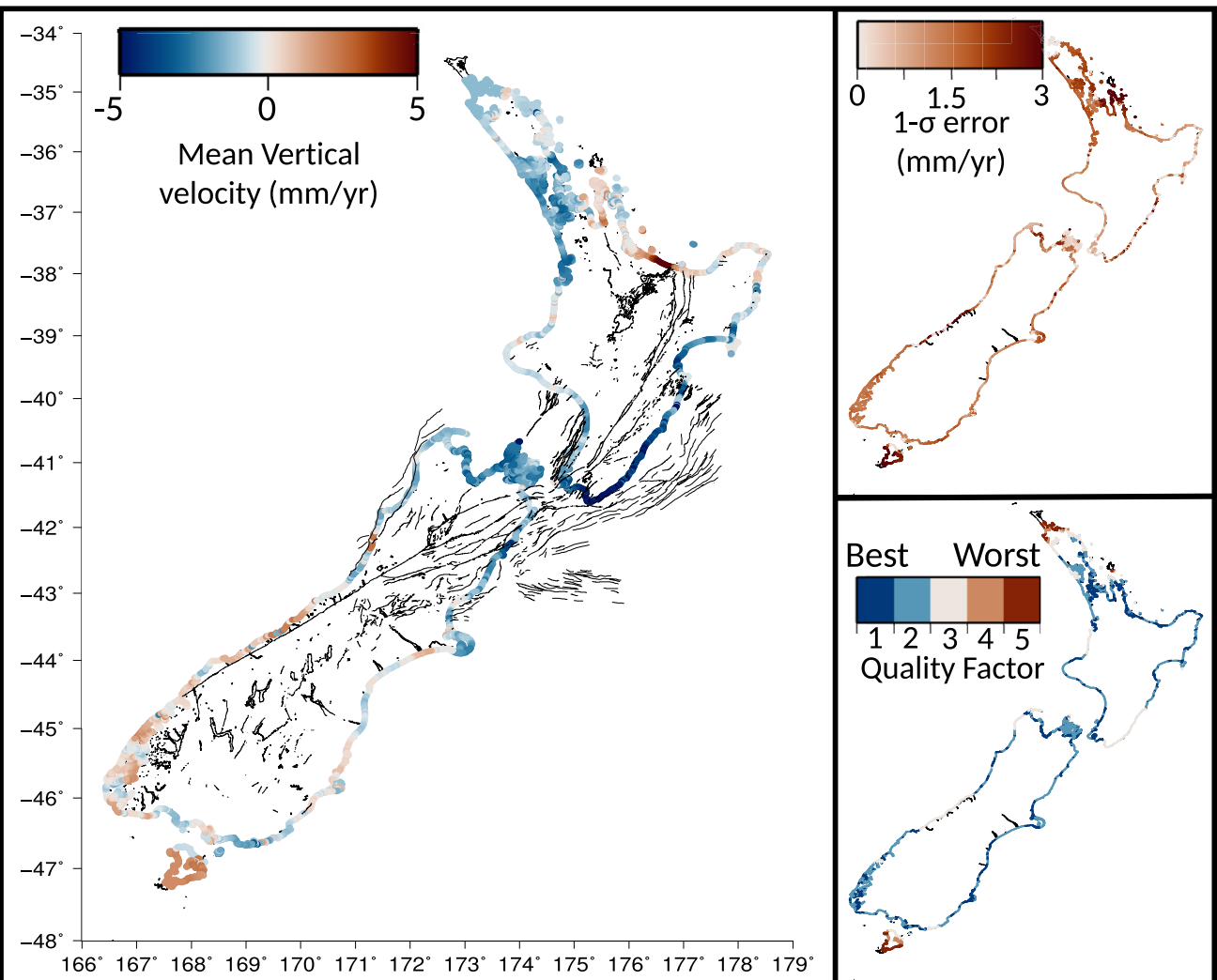


Figure 4. The main figure shows the VLM for the New Zealand coastline. The two panels on the right show the $1-\sigma$ uncertainties and the quality factor (Table S1 in Supporting Information S1).

immediately clear, based on the spatial distribution of the subsiding regions it is possible that it is related to the compaction of the sediment load after abandonment of the river channel (Higgins et al., 2014; Zhang et al., 2015).

Limited numbers of continuous GNSS across the South Island make resolving the vertical component of the deformation challenging. Previous estimates suggest generally low magnitudes of vertical deformation across much of the South Island at rates of $\sim \pm 1\text{--}2$ mm/yr (Houlié & Stern, 2017). The InSAR derived rates also suggest overall low rates. Across some of the more agricultural areas to the east of the Alps, there is a tendency toward slight subsidence (Figure 1). There is also some focused subsidence through the city of Dunedin associated with zones of reclaimed land. Across the central Alps, which GNSS suggests is uplifting at rates of ~ 5 mm/yr (Beavan, Denys, et al., 2010), the InSAR derived uplift rates give similar values of $\sim 4\text{--}5$ mm/yr (Figure 2) but are limited by the poor distribution of scatterers and non-tectonic signals (Figure 3).

One of the ongoing debates around the Kaikōura earthquake relates to the involvement of the southern portion of the Hikurangi subduction zone (Bai et al., 2017; Clark et al., 2017; Hamling et al., 2017; Hamling, 2020; Hollingsworth et al., 2017; T. Wang et al., 2018). Prior to the earthquake, studies based on seismological indicators suggested that the subduction interface south of the Cook Strait was permanently locked (Reyners et al., 1997, 2017). Although estimates of the amount of slip vary, most of the co-seismic models suggest that there was at least some co-seismic slip along the subduction interface beneath the northern South Island (Bai et al., 2017; Clark

et al., 2017; Hamling et al., 2017; Hamling, 2020; Hollingsworth et al., 2017; T. Wang et al., 2018). Furthermore, early post-seismic deformation (Mouslopoulou et al., 2019; Wallace et al., 2018) was consistent with afterslip (and/or triggered slip) along the subduction interface. Long term geological strain rates across the northern South Island (Holt & Haines, 1995) show that the majority of the relative plate motion is accommodated via deformation of the overriding plate. Elastic block models based on horizontal GNSS velocities and fault slip rate data indicate that ~80% of the plate motion is taken up by known crustal faults (Wallace, Barnes, et al., 2012; Wallace et al., 2018) with a remaining component on the subduction interface and suggest at least partial locking of the southern portion of the subduction zone. Simple elastic back-slip models (Kanda & Simons, 2010; Savage, 1983) produce downward tilting toward the trench during the interseismic period. Although smaller in magnitude than in the southern North Island, both the InSAR and GNSS show a narrow (~15–20 km) band of coastal subsidence of 1–3 mm/yr consistent with partial locking of the interface (Figures 1, 2, and 4; Wallace, Barnes, et al., 2012) in the decades prior to the Kaikōura earthquake.

4. Nationwide Coastal VLM

With sea levels rising globally, the ability to measure the vertical land movements (VLMs) and its effect on relative sea-level rise around our coastlines are vital in assessing its future impacts (Blackwell et al., 2020). With 15,000 km of coast, measuring the VLM across New Zealand's entire coastline through traditional approaches, such as with sparsely distributed GNSS, is challenging. However, based on our vertical estimate of the velocity field by combining InSAR and GNSS, we can provide a first, almost continuous, estimate of the coastal VLM. To extract the coastal strip, we bin and average all of the InSAR and GNSS observations which are located within 5 km of the coast at ~1 km intervals. Unfortunately, due to lack of coverage in some areas there are not always sufficient data points located within 5 km of the coast. For these locations, we expand the search radius up to a maximum of 40 km to estimate the VLM. In addition to the formal error of the displacement rate, we also produce a quality factor which is based on the number of observations available for each coastal location and the radial distance used to bin the observations over (Figure 4 and Table S1 in Supporting Information S1). Locations with large numbers of observations and a smaller radius have a higher ranking than those with fewer data points and larger search radii (Table S1 in Supporting Information S1). For example, points located at the northern tip of Northland, where there are not any InSAR observations, the coastal VLM is estimated purely from a single GNSS site giving it a low quality factor despite the low formal uncertainty in the measurement.

A major challenge for estimating the long-term VLM for New Zealand is its dynamic tectonic and volcanic setting. While the Envisat data presented here spans a time period where New Zealand was relatively unaffected by earthquakes, areas of coastline are not stable through time. The uplift across the Bay of Plenty reached rates of ~10 mm/yr during the observation period. However, GNSS now shows much lower levels of uplift. Similarly, the majority of the east coast margin is currently experiencing subsidence of ~5 mm/yr but is largely a result of coupling along the plate interface. Assuming that in the future there will be a rupture along the margin, this pattern of subsidence will likely be reversed as was seen during the Kaikōura earthquake in 2016. There, the coastline was subsiding at rates of ~2–3 mm/yr but was uplifted by 3–10 m by the co-seismic deformation (Hamling et al., 2017) causing long-term changes to the coast.

5. Conclusions

Using GNSS and archived Envisat SAR data acquired between 2003 and 2011, we have generated a new InSAR-based velocity field for New Zealand. By removing the expected horizontal velocities, we have produced a nationwide estimate of the vertical deformation field for the first time. Despite data limitations, the estimated vertical rates show large variability around the country as a result of volcanic, tectonic, and anthropogenic sources. Large scale subsidence across the North Island's east coast associated with locking of the Hikurangi margin appears to extend into the northern South Island supporting previous observations of partial locking of the subduction zone beneath Kaikōura (Wallace, Barnes, et al., 2012). Exploiting the vertical rates, we have produced a map of coastal VLM which can be integrated into sea level rise predictions. The large volumes of SAR data now being acquired through different satellite missions will enable regular updates of deformation fields, feeding into nationwide strain mapping (Haines & Wallace, 2020; Weiss et al., 2020) and aiding in estimates of coastal VLMs.

Data Availability Statement

The authors would like to thank the European Space Agency for access to archived Envisat data over New Zealand. The full resolution InSAR velocities and coastal VLM is available from <https://data.gns.cri.nz/metadata/srv/eng/catalog.search#/metadata/fdbb8847-c882-4324-ae48-ca7ed9b7433b> (DOI:<https://doi.org/10.21420/E1C1-MQ19>).

Acknowledgments

This work was supported by Marsden Fast Start Grant 1602 to IJH, the Ministry of Business, Innovation and Employment NZ SeaRise project, public research funding from the Government of New Zealand and the Centre for the Observation and Modelling of Earthquakes, Volcanoes and Tectonics (COMET).

References

- Bai, Y., Lay, T., Cheung, K. F., & Ye, L. (2017). Two regions of seafloor deformation generated the tsunami for the 13 November 2016, Kaikoura, New Zealand earthquake. *Geophysical Research Letters*, 44(13), 6597–6606. <https://doi.org/10.1002/2017gl073717>
- Beavan, J., Denys, P., Denham, M., Hager, B., Herring, T., & Molnar, P. (2010). Distribution of present-day vertical deformation across the Southern Alps, New Zealand, from 10 years of GPS data. *Geophysical Research Letters*, 37(16). <https://doi.org/10.1029/2010gl044165>
- Beavan, J., & Haines, J. (2001). Contemporary horizontal velocity and strain rate fields of the Pacific-Australian plate boundary zone through New Zealand. *Journal of Geophysical Research: Solid Earth*, 106(B1), 741–770. <https://doi.org/10.1029/2000jb900302>
- Beavan, J., Moore, M., Pearson, C., Henderson, M., Parsons, B., Bourne, S., et al. (1999). Crustal deformation during 1994–1998 due to oblique continental collision in the central Southern Alps, New Zealand, and implications for seismic potential of the Alpine fault. *Journal of Geophysical Research: Solid Earth*, 104(B11), 25233–25255. <https://doi.org/10.1029/1999jb900198>
- Beavan, J., Motagh, M., Fielding, E. J., Donnelly, N., & Collett, D. (2012). Fault slip models of the 2010–2011 Canterbury, New Zealand, earthquakes from geodetic data and observations of postseismic ground deformation. *New Zealand Journal of Geology and Geophysics*, 55(3), 207–221. <https://doi.org/10.1080/00288306.2012.697472>
- Beavan, J., Samsonov, S., Denys, P., Sutherland, R., Palmer, N., & Denham, M. (2010). Oblique slip on the Puysegur subduction interface in the 2009 July Mw 7.8 Dusky Sound earthquake from GPS and InSAR observations: Implications for the tectonics of southwestern New Zealand. *Geophysical Journal International*, 183(3), 1265–1286. <https://doi.org/10.1111/j.1365-246x.2010.04798.x>
- Beavan, J., Wallace, L. M., Palmer, N., Denys, P., Ellis, S., Fournier, N., et al. (2016). New Zealand GPS velocity field: 1995–2013. *New Zealand Journal of Geology and Geophysics*, 59(1), 5–14. <https://doi.org/10.1080/00288306.2015.1112817>
- Biggs, J., & Wright, T. J. (2020). How satellite InSAR has grown from opportunistic science to routine monitoring over the last decade. *Nature Communications*, 11(1), 1–4. <https://doi.org/10.1038/s41467-020-17587-6>
- Blackwell, E., Shirzaei, M., Ojha, C., & Werth, S. (2020). Tracking California's sinking coast from space: Implications for relative sea-level rise. *Science Advances*, 6(31), eaba4551. <https://doi.org/10.1126/sciadv.aba4551>
- Cavalié, O., Lasserre, C., Doin, M.-P., Peltzer, G., Sun, J., Xu, X., & Shen, Z.-K. (2008). Measurement of interseismic strain across the Haiyuan fault (Gansu, China), by InSAR. *Earth and Planetary Science Letters*, 275(3–4), 246–257. <https://doi.org/10.1016/j.epsl.2008.07.057>
- Clark, K., Nissen, E., Howarth, J., Hamling, I., Mountjoy, J., Ries, W., et al. (2017). Highly variable coastal deformation in the 2016 Mw 7.8 Kaikōura earthquake reflects rupture complexity along a transpressional plate boundary. *Earth and Planetary Science Letters*, 474, 334–344. <https://doi.org/10.1016/j.epsl.2017.06.048>
- Dimitrova, L., Wallace, L., Haines, A., & Williams, C. (2016). High-resolution view of active tectonic deformation along the Hikurangi subduction margin and the Taupo Volcanic Zone, New Zealand. *New Zealand Journal of Geology and Geophysics*, 59(1), 43–57. <https://doi.org/10.1080/00288306.2015.1127823>
- Ebmeier, S., Andrews, B., Araya, M., Arnold, D., Biggs, J., Cooper, C., et al. (2018). Synthesis of global satellite observations of magmatic and volcanic deformation: Implications for volcano monitoring & the lateral extent of magmatic domains. *Journal of Applied Volcanology*, 7(1), 1–26. <https://doi.org/10.1186/s13617-018-0071-3>
- Farr, T. G., Rosen, P. A., Caro, E., Crippen, R., Duren, R., Hensley, S., et al. (2007). The shuttle radar topography mission. *Reviews of Geophysics*, 45(2). <https://doi.org/10.1029/2005rg000183>
- Haines, A. J., & Wallace, L. M. (2020). New Zealand-wide geodetic strain rates using a physics-based approach. *Geophysical Research Letters*, 47(1), e2019GL084606. <https://doi.org/10.1029/2019gl084606>
- Hamling, I. J. (2020). A review of the 2016 Kaikōura earthquake: Insights from the first 3 years. *Journal of the Royal Society of New Zealand*, 50(2), 226–244. <https://doi.org/10.1080/03036758.2019.1701048>
- Hamling, I. J., Cevard, S., & Garaebiti, E. (2019). Large-scale drainage of a complex magmatic system: Observations from the 2018 Eruption of Ambrym Volcano, Vanuatu. *Geophysical Research Letters*, 46(9), 4609–4617. <https://doi.org/10.1029/2019gl082606>
- Hamling, I. J., D'Anastasio, E., Wallace, L., Ellis, S., Motagh, M., Samsonov, S., et al. (2014). Crustal deformation and stress transfer during a propagating earthquake sequence: The 2013 Cook Strait sequence, central New Zealand. *Journal of Geophysical Research: Solid Earth*, 119(7), 6080–6092. <https://doi.org/10.1002/2014jb011084>
- Hamling, I. J., & Hreinsdóttir, S. (2016). Reactivated afterslip induced by a large regional earthquake, Fiordland, New Zealand. *Geophysical Research Letters*, 43(6), 2526–2533. <https://doi.org/10.1002/2016gl067866>
- Hamling, I. J., Hreinsdóttir, S., Bannister, S., & Palmer, N. (2016). Off-axis magmatism along a subaerial back-arc rift: Observations from the Taupo Volcanic Zone, New Zealand. *Science Advances*, 2(6), e1600288. <https://doi.org/10.1126/sciadv.1600288>
- Hamling, I. J., Hreinsdóttir, S., Clark, K., Elliott, J., Liang, C., Fielding, E., & Stirling, M. (2017). Complex multifault rupture during the 2016 Mw 7.8 Kaikōura earthquake, New Zealand. *Science*, 356(6334), eaam7194. <https://doi.org/10.1126/science.aam7194>
- Hamling, I. J., Hreinsdóttir, S., & Fournier, N. (2015). The ups and downs of the TVZ: Geodetic observations of deformation around the Taupo volcanic zone, New Zealand. *Journal of Geophysical Research: Solid Earth*, 120(6), 4667–4679. <https://doi.org/10.1002/2015jb012125>
- Hamling, I. J., & Wallace, L. M. (2015). Silent triggering: Aseismic crustal faulting induced by a subduction slow slip event. *Earth and Planetary Science Letters*, 421, 13–19. <https://doi.org/10.1016/j.epsl.2015.03.046>
- Higgins, S. A., Overeem, I., Steckler, M. S., Syvitski, J. P., Seeger, L., & Akhter, S. H. (2014). InSAR measurements of compaction and subsidence in the Ganges-Brahmaputra Delta, Bangladesh. *Journal of Geophysical Research: Earth Surface*, 119(8), 1768–1781. <https://doi.org/10.1002/2014jf003117>
- Holden, L., Wallace, L., Beavan, J., Fournier, N., Cas, R., Ailleres, L., & Silcock, D. (2015). Contemporary ground deformation in the Taupo Rift and Okataina Volcanic Centre from 1998 to 2011, measured using GPS. *Geophysical Journal International*, 202(3), 2082–2105. <https://doi.org/10.1093/gji/ggv243>
- Hollingsworth, J., Ye, L., & Avouac, J.-P. (2017). Dynamically triggered slip on a splay fault in the Mw 7.8, 2016 Kaikoura (New Zealand) earthquake. *Geophysical Research Letters*, 44(8), 3517–3525. <https://doi.org/10.1002/2016gl072228>

- Holt, W. E., & Haines, A. (1995). The kinematics of northern South Island, New Zealand, determined from geologic strain rates. *Journal of Geophysical Research: Solid Earth*, 100(B9), 17991–18010. <https://doi.org/10.1029/95jb01059>
- Hooper, A. (2008). A multi-temporal InSAR method incorporating both persistent scatterer and small baseline approaches. *Geophysical Research Letters*, 35(16). <https://doi.org/10.1029/2008gl034654>
- Hooper, A., Bekaert, D., Spaans, K., & Arkan, M. (2012). Recent advances in SAR interferometry time series analysis for measuring crustal deformation. *Tectonophysics*, 514, 1–13. <https://doi.org/10.1016/j.tecto.2011.10.013>
- Houlié, N., & Stern, T. A. (2017). Vertical tectonics at an active continental margin. *Earth and Planetary Science Letters*, 457, 292–301. <https://doi.org/10.1016/j.epsl.2016.10.018>
- Hussain, E., Hooper, A., Wright, T. J., Walters, R. J., & Bekaert, D. P. (2016). Interseismic strain accumulation across the central North Anatolian Fault from iteratively unwrapped InSAR measurements. *Journal of Geophysical Research: Solid Earth*, 121(12), 9000–9019. <https://doi.org/10.1002/2016jb013108>
- Kampes, B. M., Hanssen, R. F., & Perski, Z. (2003). Radar interferometry with public domain tools. In *Proceedings of fringe* (pp. 1–5).
- Kanda, R. V., & Simons, M. (2010). An elastic plate model for interseismic deformation in subduction zones. *Journal of Geophysical Research*, 115(B3). <https://doi.org/10.1029/2009jb006611>
- Lamb, S., Moore, J. D., Smith, E., & Stern, T. (2017). Episodic kinematics in continental rifts modulated by changes in mantle melt fraction. *Nature*, 547(7661), 84–88. <https://doi.org/10.1038/nature22962>
- Langridge, R., & Berryman, K. (2005). Morphology and slip rate of the Hurunui section of the Hope Fault, South Island, New Zealand. *New Zealand Journal of Geology and Geophysics*, 48(1), 43–57. <https://doi.org/10.1080/00288306.2005.9515097>
- Langridge, R., Ries, W., Litchfield, N., Villamor, P., Van Dissen, R., Barrell, D., et al. (2016). The New Zealand active faults database. *New Zealand Journal of Geology and Geophysics*, 59(1), 86–96. <https://doi.org/10.1080/00288306.2015.1112818>
- Little, T. A., Cox, S., Vry, J. K., & Batt, G. (2005). Variations in exhumation level and uplift rate along the oblique-slip Alpine fault, central Southern Alps, New Zealand. *The Geological Society of America Bulletin*, 117(5–6), 707–723. <https://doi.org/10.1130/b25500.1>
- Michailos, K., Sutherland, R., Townend, J., & Savage, M. K. (2020). Crustal thermal structure and exhumation rates in the Southern Alps near the Central Alpine Fault, New Zealand. *Geochemistry, Geophysics, Geosystems*, 21(8), e2020GC008972. <https://doi.org/10.1029/2020gc008972>
- Mouslopoulou, V., Saltogianni, V., Nicol, A., Oncken, O., Begg, J., Babeyko, A., et al. (2019). Breaking a subduction-termination from top to bottom: The large 2016 Kaikoura Earthquake, New Zealand. *Earth and Planetary Science Letters*, 506, 221–230. <https://doi.org/10.1016/j.epsl.2018.10.020>
- Nicol, A., & Beavan, J. (2003). Shortening of an overriding plate and its implications for slip on a subduction thrust, central Hikurangi Margin, New Zealand. *Tectonics*, 22(6). <https://doi.org/10.1029/2003tc001521>
- Norris, R. J., & Cooper, A. F. (2001). Late Quaternary slip rates and slip partitioning on the Alpine Fault, New Zealand. *Journal of Structural Geology*, 23(2), 507–520. [https://doi.org/10.1016/s0191-8141\(00\)00122-x](https://doi.org/10.1016/s0191-8141(00)00122-x)
- Pritchard, M. E., & Simons, M. (2002). A satellite geodetic survey of large-scale deformation of volcanic centres in the central Andes. *Nature*, 418(6894), 167–171. <https://doi.org/10.1038/nature00872>
- Reyners, M., Eberhart-Phillips, D., & Bannister, S. (2017). Subducting an old subduction zone sideways provides insights into what controls plate coupling. *Earth and Planetary Science Letters*, 466, 53–61. <https://doi.org/10.1016/j.epsl.2017.03.004>
- Reyners, M., McGinty, P., Cox, S., Turnbull, I., Gledhill, K., Hancox, G., et al. (2003). The Mw 7.2 Fiordland earthquake of August 21, 2003: Background and preliminary results. *Bulletin-New Zealand Society for Earthquake Engineering*, 36(4), 233–248. <https://doi.org/10.5459/bnzsee.36.4.233-248>
- Reyners, M., Robinson, R., & McGinty, P. (1997). Plate coupling in the northern South Island and southernmost North Island, New Zealand, as illuminated by earthquake focal mechanisms. *Journal of Geophysical Research: Solid Earth*, 102(B7), 15197–15210. <https://doi.org/10.1029/97jb00973>
- Rosen, P. A., Hensley, S., Peltzer, G., & Simons, M. (2004). Updated repeat orbit interferometry package released. *Eos, Transactions, American Geophysical Union*, 85(5), 35. <https://doi.org/10.1029/2004eo050004>
- Savage, J. C. (1983). A dislocation model of strain accumulation and release at a subduction zone. *Journal of Geophysical Research: Solid Earth*, 88(B6), 4984–4996. <https://doi.org/10.1029/jb088ib06p04984>
- Sutherland, R., Berryman, K., & Norris, R. (2006). Quaternary slip rate and geomorphology of the Alpine fault: Implications for kinematics and seismic hazard in southwest New Zealand. *The Geological Society of America Bulletin*, 118(3–4), 464–474. <https://doi.org/10.1130/b25627.1>
- Upton, P., & Koons, P. O. (2007). Three-dimensional geodynamic framework for the Central Southern Alps, New Zealand: Integrating geology, geophysics and mechanical observations. *Geophysical Monograph Series*, 175, 253–270. <https://doi.org/10.1029/175gm13>
- Upton, P., Koons, P. O., Craw, D., Henderson, C. M., & Enlow, R. (2009). Along-strike differences in the Southern Alps of New Zealand: Consequences of inherited variation in rheology. *Tectonics*, 28(2). <https://doi.org/10.1029/2008tc002353>
- Van Dissen, R., & Yeats, R. S. (1991). Hope fault, Jordan thrust, and uplift of the seaward Kaikoura Range, New Zealand. *Geology*, 19(4), 393–396. [https://doi.org/10.1130/0091-7613\(1991\)019<0393:hftau>2.3.co;2](https://doi.org/10.1130/0091-7613(1991)019<0393:hftau>2.3.co;2)
- Wallace, L. M. (2020). Slow slip events in New Zealand. *Annual Review of Earth and Planetary Sciences*, 48, 175–203. <https://doi.org/10.1146/annurev-earth-071719-055104>
- Wallace, L. M., Barnes, P., Beavan, J., Van Dissen, R., Litchfield, N., Mountjoy, J., & Pondard, N. (2012). The kinematics of a transition from subduction to strike-slip: An example from the central New Zealand plate boundary. *Journal of Geophysical Research: Solid Earth*(B2), 117. <https://doi.org/10.1029/2011jb008640>
- Wallace, L. M., & Beavan, J. (2010). Diverse slow slip behavior at the Hikurangi subduction margin, New Zealand. *Journal of Geophysical Research: Solid Earth*(B12), 115. <https://doi.org/10.1029/2010jb007717>
- Wallace, L. M., Beavan, J., Bannister, S., & Williams, C. (2012). Simultaneous long-term and short-term slow slip events at the Hikurangi subduction margin, New Zealand: Implications for processes that control slow slip event occurrence, duration, and migration. *Journal of Geophysical Research*, (B11), 117. <https://doi.org/10.1029/2012jb009489>
- Wallace, L. M., Beavan, J., McCaffrey, R., Berryman, K., & Denys, P. (2007). Balancing the plate motion budget in the South Island, New Zealand using GPS, geological and seismological data. *Geophysical Journal International*, 168(1), 332–352. <https://doi.org/10.1111/j.1365-246x.2006.03183.x>
- Wallace, L. M., Beavan, J., McCaffrey, R., & Darby, D. (2004). Subduction zone coupling and tectonic block rotations in the North Island, New Zealand. *Journal of Geophysical Research*, 109(B12), B12406. <https://doi.org/10.1029/2004jb003241>
- Wallace, L. M., Hreinsdóttir, S., Ellis, S., Hamling, I., D'Anastasio, E., & Denys, P. (2018). Triggered slow slip and afterslip on the southern hikurangi subduction zone following the kaikoura earthquake. *Geophysical Research Letters*, 45, 4710–4718.
- Wang, H., Wright, T. J., Yu, Y., Lin, H., Jiang, L., Li, C., & Qiu, G. (2012). InSAR reveals coastal subsidence in the Pearl River Delta, China. *Geophysical Journal International*, 191(3), 1119–1128. <https://doi.org/10.1111/j.1365-246x.2012.05687.x>

- Wang, T., Wei, S., Shi, X., Qiu, Q., Li, L., Peng, D., et al. (2018). The 2016 Kaikōura earthquake: Simultaneous rupture of the subduction interface and overlying faults. *Earth and Planetary Science Letters*, 482, 44–51. <https://doi.org/10.1016/j.epsl.2017.10.056>
- Weiss, J. R., Walters, R. J., Morishita, Y., Wright, T. J., Lazecky, M., Wang, H., et al. (2020). High-resolution surface velocities and strain for Anatolia from Sentinel-1 InSAR and GNSS data. *Geophysical Research Letters*, 47(17), e2020GL087376. <https://doi.org/10.1029/2020GL087376>
- Zhang, J.-Z., Huang, H.-J., & Bi, H.-B. (2015). Land subsidence in the modern Yellow River Delta based on InSAR time series analysis. *Natural Hazards*, 75(3), 2385–2397. <https://doi.org/10.1007/s11069-014-1434-7>